JOURNAL OF GEOPHYSICAL RESEARCH, VOL. 113, C12026, doi:10.1029/2007JC004155, 2008

Topographic effects on the path and evolution of Loop Current Eddies

Kyung Hoon Hyun[1,2] and Patrick J. Hogan[3]

Received 12 February 2007; revised 12 August 2008; accepted 2 September 2008; published 30 December 2008.

[1] Eddy-topography (ET) interactions are important in determining the path and evolution of oceanic eddies, including Loop Current Eddies (LCE) in the Gulf of Mexico (GOM). We use the Hybrid Coordinate Ocean Model and satellite altimetry data to investigate the ET interactions and the impact on LCE pathway evolution in the GOM. Satellite altimetry reveals that LCEs translate dominantly westward in the central GOM and strongly collide and reflect against topography near the continental slope in the northern and western GOM. The result is the frequent generation of an anticyclone-cyclone (AC) pair in conjunction with the LCEs. In the absence of lateral or surface boundary forcing but including realistic topography, simulations initialized with idealized eddies at various locations in the GOM reveal the following results. Southward eddy reflection from the northern slope occurs when a cyclone drastically strengthens east of the anticyclone because of the ET collision. The prevailing westward propagation in the central GOM occurs because the cyclone is very dispersive toward nearby topographic features, causing a reduced southward component of drift and/or moves to the south, forming a meridional AC pair, causing an enhanced westward component. ET collision is strongest over the northwestern slope (north of 24°N) because of the eddy colliding relatively normal to the steep slope, and the eddy typically tracks anticyclonic pathways during the collision/reflection process. Along the western slope, a strong ET collision produces a southeastward reflection, and the accompanying cyclone to the northeast strongly enhances the reflection. Near the southern GOM slope, eddy pathways tend to propagate alongslope with an onshore-offshore oscillatory trajectory because of the competition between topographic and planetary β effects. In the southwestern GOM a bimodal pathway occurs, i.e., northward migration with an anticyclonic route for relatively stronger eddies and southward dissipative propagation along the shelf edge for weaker ones.

Citation: Hyun, K. H., and P. J. Hogan (2008), Topographic effects on the path and evolution of Loop Current Eddies, *J. Geophys. Res.*, *113*, C12026, doi:10.1029/2007JC004155.

1. Introduction

[2] The dominant circulation feature in the Gulf of Mexico (GOM) is the Loop Current Extension and Loop Current Eddies (LCE) which quasi-periodically shed from the Loop Current and propagate predominantly westward. This Loop Current system is driven by inflow through the Yucatan Straits and outflow through the Florida Straits, resulting in the transport of a large volume of Caribbean-origin water to the western GOM, ultimately interacting with continental slope along the Mexican-U.S. coastal regions [cf. *Sturges and Lugo-Fernandez*, 2005; *Vidal et al.*, 1992]. Loop Current Eddies are one of the largest eddies (~300 km diameter) which experience a strong eddy-topography (ET) collision/interaction with a steep western continental slope within a comparatively short period from generation (3–6 months) without dissipating much by interactions with a strong jet or other eddies. During the LCE-topography collisions, generation of relatively strong slope jets and cross-slope currents as well as many "slope-induced" eddies has been observed [*Vukovich and Waddell*, 1991; *Nowlin et al.*, 2005]. Although several numerical studies of the GOM have simulated the Loop Current system quite well [e.g., *Hurlburt and Thompson*, 1982; *Lee and Mellor*, 2003; *Chassignet et al.*, 2005], studies on LCE-topography collision/interaction are relatively sparse.

[3] Using a satellite-tracked drifting buoy and hydrographic data, *Vukovich and Waddell* [1991] reported on the behavior of an LCE interacting with the continental slope in the western GOM. They noted that the LCE experienced distortion (circular to elliptic), clockwise rotation of its axis, and southeastward propagation after the LCE collided with the continental slope. *Hamilton et al.* [1999] also used drifter and hydrographic data to suggest a mean propagation pathway for LCEs in general. In the northwestern GOM, northwestward translation and northeastward reflection have been frequently observed near the continental slope [e.g., *Vukovich*, 2005], opposite that of the

[1]Department of Marine Sciences, University of Southern Mississippi, Hattiesburg, Mississippi, USA.
[2]Now at Department of Marine, Earth, and Atmospheric Sciences, North Carolina State University, Raleigh, North Carolina, USA.
[3]Naval Research Laboratory, Stennis Space Center, Mississippi, USA.

0148-0227/08/2007JC004155$09.00

conventional southwestward path. Indeed, on the basis of various observations, LCEs that collided with the continental slope in the western GOM have been shown to propagate northward, southward, or eastward [i.e., *Vukovich and Crissman*, 1986; *Kirwan et al.*, 1988; *Hamilton et al.*, 1999]. A key question is what mechanisms determine the propagation pathway after collision with the continental slope.

[4] Numerical models have been widely used in studies of understanding the interactions between eddies (usually anticyclones) and topography, including *Nof* [1983], *Smith and O'Brien* [1983], *Mory et al.* [1987], *Grimshaw et al.* [1994], *Thierry and Morel* [1999], and *Sansón and van Heijst* [2000]. Other specific studies include eddy "reflection" due to LCE-topography interaction [*Smith*, 1986], the effect of western "wall" boundaries [*Shi and Nof*, 1993; *Nof*, 1999], the effect of slope width on eddy propagation [*Frolov et al.*, 2004a, 2004b] and the response of a cyclone to topography with an f-plane [*LaCasce*, 1998]. *Jacob et al.* [2002] investigated whether the baroclinicity/barotropy associated with LCEs affected eddy-topography (ET) interactions, including topographic orientations, and suggested that eddy propagation over a slope strongly depended on the barotropy of the eddy, in addition to the orientation and steepness of the slope. *Oey and Zhang* [2004] reported the generation of cyclones and a slope jet on the convergent side of a warm eddy colliding with the continental slope on the northern GOM and its adjacent shelf. *Herbette et al.* [2003, 2005] investigated eddy erosion over a seamount using model on f- and β-planes and suggested that the deep fluid motions induced by the initial eddy across potential vorticity gradients played a major role in the eddy erosion. *Hyun and Hogan* [2008] (hereinafter referred to as HH) investigated the effects of slope steepness and orientation on the anticyclone evolution using the Hybrid Coordinate Ocean Model (HYCOM), and suggested that along slope eddy deflection increased as the steepness increased, generating a "collision" cyclone and a slope jet to the south of the anticyclone, and that the anticyclone translation was strongly affected by the location of adjacent cyclones.

[5] Since the western GOM is bounded by continental slopes to the north, south, and west, and the orientation of the slopes have a large impact on eddy propagation [*Jacob et al.*, 2002; HH], the initial eddy impact point is critical to LCE-topography interaction. This study is extended from previous studies [e.g., *Jacob et al.*, 2002; *Sutyrin et al.*, 2003; *Frolov et al.*, 2004a; *Oey and Zhang*, 2004; HH] in integration time (weeks, months to years), from idealized to realistic GOM/slope bathymetry, extension from the f-plane approximation to β-plane, and in consideration of eddy-topography interactions on all continental slopes (i.e., northern, southern, and western). Major research questions include how/why LCEs propagate along specific pathways in the central and western GOM depending on their geographical location in the model initial state and how eddy-topography collisions affect evolution of individual eddy pathways. Results from these idealized eddy simulations are compared to observations from satellite altimetry and a high-resolution GOM model that includes realistic lateral and surface boundary forcing.

[6] The remainder of the paper is organized as follows: Section 2 describes satellite altimetry data and HYCOM model configuration. Okubo-Weiss parameter for eddy tracking and nondimensional eddy property numbers are also described. Section 3.1 describes typical examples of LCE pathway migration and LCE-topography interaction as observed in satellite altimetry. The pathway and evolution of isolated anticyclones from model simulations, including interactions with northern/southern/western continental slopes are presented in section 3.2. Section 3.3 presents results from a realistic GOM circulation model, followed by a summary in section 4.

2. Data and Model

[7] The Modular Ocean Data Assimilation System (MODAS) and the Hybrid Coordinate Ocean Model (HYCOM) are the primary tools used in this study. MODAS is a modular toolkit used to depict and predict the three-dimensional temperature and salinity structure for the global ocean, often in areas where little if any in situ data are available. It relies heavily on remotely sensed surface observations and statistical regression techniques to estimate the subsurface thermal structure. For details of MODAS, refer to *Fox et al.* [2002a, 2002b] and the Web site http://www.7320.nrlssc.navy.mil/modas. MODAS Sea level anomaly (SLA) covering the time period 1993–2007 with a horizontal resolution of 1/8° are used in this study. SLA and Okubo-Weiss parameter W [*Okubo*, 1970; *Weiss*, 1991; *Isern-Fontanet et al.*, 2004] are employed to track the center of observed Loop Current Eddies (see Figures 4, 5, and 6). W is defined as

$$W = s_n^2 + s_s^2 + \omega^2, \tag{1}$$

where the normal and shear components of strain s_n, s_s and the relative vorticity of flow ω are defined as

$$s_n = u_x - v_y, s_s = v_x + u_y, \omega = v_x - u_y,$$

where subscripts denote partial differentiation and u and v are defined horizontal currents assuming geostrophic balance as

$$u = -\frac{g}{f_0}\frac{\partial h'}{\partial y}, v = \frac{g}{f_0}\frac{\partial h'}{\partial x},$$

where h' is the sea level anomaly, g is the gravitational acceleration and f_0 is the Coriolis parameter (7.0×10^{-5} s^{-1}).

[8] HYCOM is an advanced ocean circulation model which continually seeks an appropriate vertical scheme from three choices, z-level, terrain-following and isopycnic coordinates [*Bleck and Boudra*, 1981]. It was originally designed for the accurate transition from the deep water to the shallow water. It has been widely applied to simulate the regional and large-scale ocean circulation [*Hogan and Hurlburt*, 2006; *Chassignet et al.*, 2003; *Prasad and Hogan*, 2007]. The GOM region with 5 min bathymetry was interpolated to the model grid with horizontal resolu-

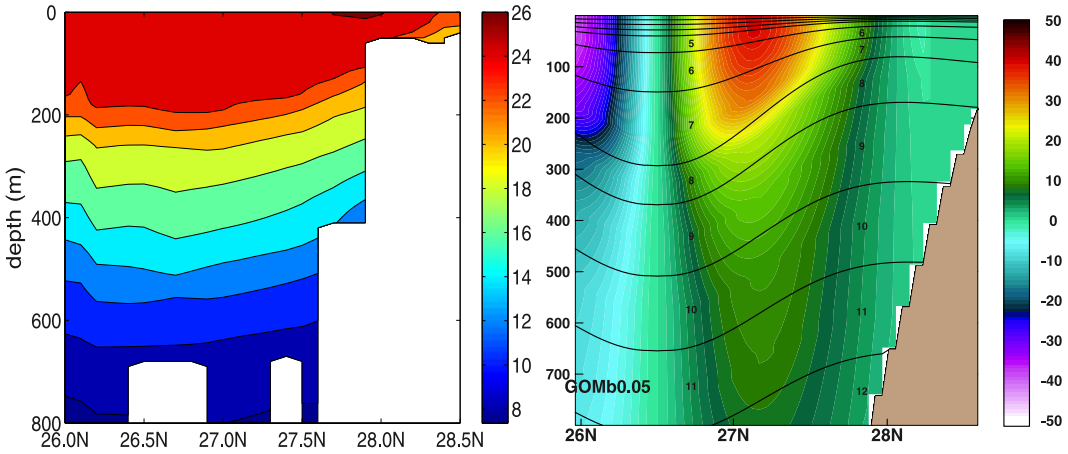

Figure 1. (a) Isotherms (°C) along a Loop Current Eddy observed in the Gulf of Mexico in April 2001 (eddy 01A in Figure 6b). Data is obtained from *Operational Oceanography Group* [2006]. (b) The model eddy structure initialized using the HYCOM model (eddy I in Figure 7). Zonal current (cm s^{-1}) and layer thickness are depicted along 90°W.

tion of 1/20° and 20 vertical layers, and the K-Profile Parameterization (KPP) turbulence model was used [*Large et al.*, 1994]. The four boundaries were closed (no-slip boundary condition) and no background ambient surface forcing was applied. Initial stratification was obtained from temperature and salinity profiles for January averaged within each layer over the GOM domain from the GDEM3 climatology [*Teague et al.*, 1990], which was spatially uniform except where the idealized eddies were initialized following the process below.

[9] Figure 1a illustrates the vertical structure of a typical LCE detected from a hydrographic survey in April 2001, which was also detected in satellite altimetry depicted in Figure 6b (denoted as eddy 01A). This eddy is relatively large with a diameter of ~350 km and deep (>1000 m) and the interface depth difference is ~250 m between the eddy center and perimeter along the isotherm of 20°C. This eddy provides the basic structure for a model eddy. A quasi-geostrophically balanced anticyclonic eddy is initialized in the GOM domain using the eddy initialization method by *Carton and McWilliams* [1989] and *Herbette et al.* [2003]. The vertical structure of the initial eddy is depicted in Figure 1b. For eddy initialization, the potential vorticity anomaly (dQ) was defined as

$$dQ_k = h_0\left[\frac{\varsigma + f}{h} - \frac{f}{h_0}\right], \tag{2}$$

where k is layer, ς is relative vorticity and h_0 is the initial layer thickness. The initial dQ of $-2f_0$ was prescribed in the upper 7 layers and zero dQ in the lower layers. There is an assumed radial distribution of dQ across the eddy, and the intensity refers to its center. The initial eddy radius (R) is 120 km and the initial surface flow is 0.4 m s^{-1}, which is weaker than the LCE in the central GOM (>1 m s^{-1}) but comparable to ~0.5 m s^{-1} in the western GOM [*Kirwan et al.*, 1988]. The eddy size and stratification were fixed except for the initial locations (details in section 3.2.1).

[10] In this paper, the following nondimensional parameters are used to interpret the dynamics. The eddy intensity number ε, the planetary β effect number α, and the eddy barotropy number δ are defined as

$$\varepsilon = \frac{\omega}{f_0}, \quad \alpha = \frac{\beta_0 R}{f_0}, \quad \delta = \frac{h_e}{h}, \tag{3}$$

where ω is the eddy angular frequency, β_0 is the planetary β (2×10^{-11} m^{-1} s^{-1}), R is the eddy radius, h_e is the reference eddy depth (layer 8 was chosen in this study) and h is the total depth where the eddy center is positioned. In addition, the topographic β effect number $\alpha_{(\tau_x,\tau_y)}$ is used i.e.,

$$\alpha_{(\tau_x,\tau_y)} = \frac{\beta_{(\tau_x,\tau_y)} R}{f_0} = \frac{f}{h}\frac{\partial h}{(\partial x, \partial y)}\frac{R}{f_0}, \tag{4}$$

where $\beta_{(\tau_x,\tau_y)}$ is the topographic β in (x, y) directions and f is the Coriolis parameter.

[11] Before using a standard eddy, four cases with various eddy sizes (R = 80–200 km, Figure 2a) and five cases with various initial eddy intensities were performed in the central GOM (Figure 2b), which showed that the translation speed increases strongly with eddy intensity [*Reznik and Grimshaw*, 2001], not with eddy size. The translation speed of the standard case (R = 120 km, $dQ = -2f_0$) is ~2.0 km d^{-1}, larger eddies (R = 160 km, 200 km, $dQ = -2f_0$) show a similar translation speed but the same size eddy with strong initial intensity (R = 120 km, $dQ = -5f_0$) has a faster speed (~3 km d^{-1}). In order to minimize the effects from transient currents caused by large eddies with a strong initial intensity near the slope and to locate an eddy as close as possible to the slope, our standard case was chosen in this study, which showed the path and evolution consistent with observed LCEs. A realistic HYCOM model simulation with 1/25° horizontal resolution and climatological boundary forcing

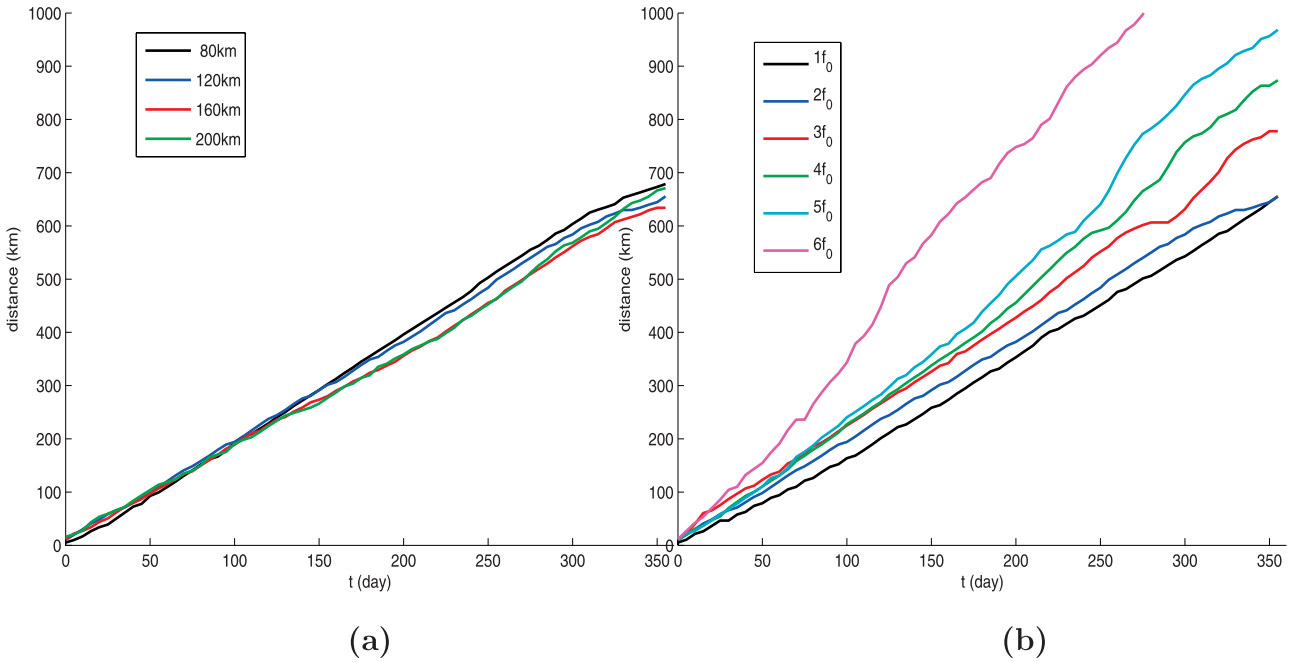

Figure 2. Eddy translation (a) by initial eddy size (R = 80–200 km) with fixed initial intensity (dQ = $-2f_0$) and (b) by initial eddy intensity (dQ = -1–$5f_0$) with fixed size (R = 120 km). The slope of curves is ~2.0 km d^{-1} for 120 km eddy (Figure 2a) and ~1.8, 2.0, 2.2, 2.4, 2.7, and 3.6 km d^{-1} for dQ = -1–$6f_0$ (Figure 2b), respectively. An eddy of 120 km radius and dQ = $-2f_0$ is chosen in this model study.

and realistic surface forcing was included to compare with idealized cases (details in section 3.3).

3. Results

3.1. Observed Path and Evolution of LCEs

[12] This section describes the path and evolution of LCEs observed from satellite altimetry data for the period of 1993–2007, and discusses ET collision/reflection and their effects on subsequent eddy evolutions. Monthly evolutions of warm-core eddies in the GOM are depicted in Figure 3. Figure 3 illustrates a synoptic view of LCE paths and behaviors in the GOM quite well, and noticeable eddy evolutions and corresponding eddy names are listed in Table 1. Even though small-scale and cyclonic eddies are not included, Figure 3 provides some insight into ET collision and topographic effects. For example, in September 1993 (orange) eddy 93A starts shedding at ~90W/26N and simultaneously another anticyclone (93B) occupies the central gulf (93W/25N). The former collides with the northern slope and turns south in December (dark red) while the latter collides with the western slope near 97W/22N. Eddy 01A in 2001 provides a very good example of eddy–northern slope collision/reflection and eddy–western slope collision/reflection (also shown in Figure 6). A total of 12 eddies experienced eddy–northern slope collision/reflection and the same number of eddies eddy–western slope collision. After the collision with the western slope, eddies are observed to migrate northward or southward. Northward migrating eddies delineate an anticyclonic route (e.g., 96A, 00C, 01A, 02A) and three eddies are clearly observed to migrate northward after ET collision at the southwestern slope (04B, 05C, 07C). Southward migrating eddies experience enhanced dissipation and distortion along the continental slope in the southwestern gulf (e.g., 93B, 95D, 99E, 00A, 02A) and are very analogous with the propagation of coastally trapped waves [*Zamudio and Hogan*, 2008]. The years 1996, 1998 and 2001 are chosen to further examine eddy evolution associated with ET collision and adjacent cyclonic/anticyclonic eddies.

[13] Figure 4 illustrates two westward translating eddies (96B, 96C) in the central GOM, and an eddy (96A) originating from the northern GOM slope. In February (Figure 4a) eddy 96B, located at 92.5W/25N and translated westward ~1.5° in January–February, drifts continuously due westward until May (Figures 4b and 4c). During the westward translation a meridional anticyclone-cyclone (AC) pair is formed. In May (Figure 4d), 96B demonstrates a northward trajectory, experiencing vortex merging with adjacent eddies to the north and south including 96C. Eddy 96C, located at 95W/23N in February (Figure 4a), demonstrates westward translation, similarly to 96B, until it collides with the western slope (96W/23N) in March (Figure 4b), subsequently merges into 96B in April (Figure 4c). On the other hand, eddy 96A begins to shed at 89W/27N near the northern slope in February (Figure 4a) and merges with an anticyclonic eddy to the south (88W/25.5N) into a stronger eddy in March (Figure 4b). In April and May (Figures 4c and 4d), this eddy translates due southward, in distinct contrast with 96B, 96C. During southward translation of 96A until May, a zonal AC pair is formed. In June (Figure 4e), 96A turns west detaching from the cyclone, and subsequently interacts with the merged anticyclone 96B. Southward translation from the northern slope is frequently observed in the GOM, and

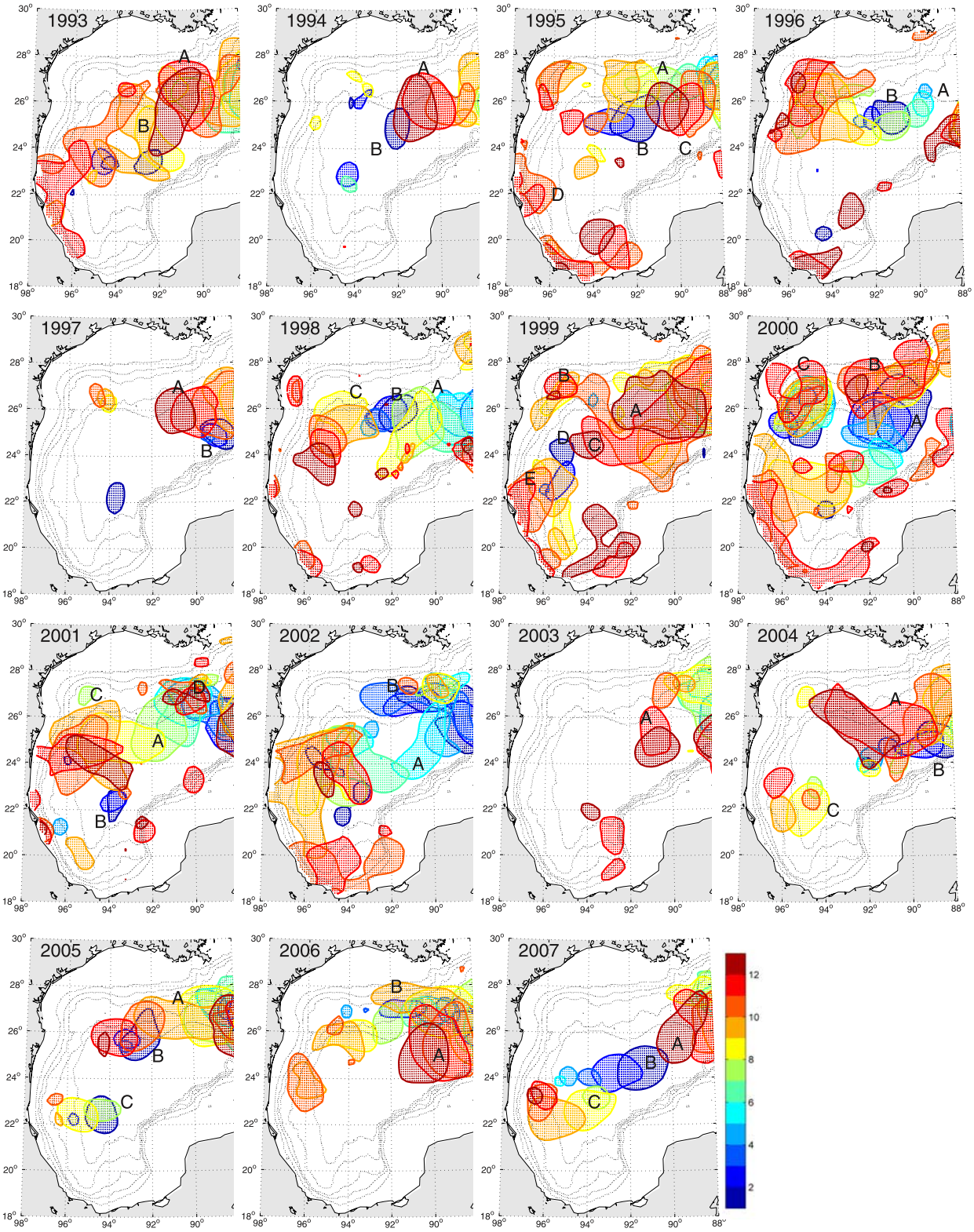

Figure 3. Monthly variation of warm-core eddies in the western Gulf of Mexico for the period of 1993–2007. The eddies are defined as sea surface height (SSH) anomaly >16 cm, of which inside area is color shaded every month. Major eddies are marked by alphabet and named such as 93A, 93B (see Table 1). Figure 3 captures a synopic view for warm-core eddy behaviors.

Table 1. Paths and Behavior of Warm Core Rings Observed in the Western Gulf of Mexico for 1993–2007 From Satellite Altimetry[a]

Warm Core Ring Path and Behavior	Warm Core Ring
Westward path in the central gulf	96A, 01A, 02A, 05A, 07B
Westward path over the northern slope	95A, 00B, 02B, 05A
Southwestward path	93B, 98A, 98C, 00A, 03A
Northern slope collision and southwest reflection	93A, 93B, 94A, 95A, 95B, 97A (98B), 98A, 01A, 02A, 03A, 04A, 05A
Northwestern slope collision and reflection	96B, 98B, 00C, 01A, 02A
Southwestern slope collision and northward migration	04B, 05C, 07C
Southwestern slope collision and collapse along the slope	93B, 95D, 99E, 00A, 02A
Southern slope collision	98A, 99A, 00A, 02A
Stationary at the northwestern slope corner	96B, 99B, 00C
Northern slope collision and reflection with a cyclone to the east	93A, 93B, 94A, 95A

[a]As shown in Figure 3.

interaction with a cyclone and the effects of ET collision are critical in this process (discussed in section 3.2.2).

[14] The merging of 96B and 96C generates a large distorted eddy in the northwestern GOM slope corner (94–96W/26–28N) in May–July (Figures 4d, 4e, and 4f), and this eddy maintains its position for more than 6 months. Three eddies were noted for similar behavior at the NW corner (96B, 99B and 00C in Figure 3 and Table 1). This phenomenon seems associated with the topographic effect of the northwest corner which forms a semienclosed slope shape between 26–28N and 94–96W, north of the slight eastward slope projection near 96W/26N. Typically eddies which have drifted toward the corner from the western or northern slopes merge at the corner. 96B is a good example of such corner-trapped eddies. Contrastingly, eddy 98C, positioned at the corner after merging with two slope eddies, is not trapped at the corner because the eddy center does not

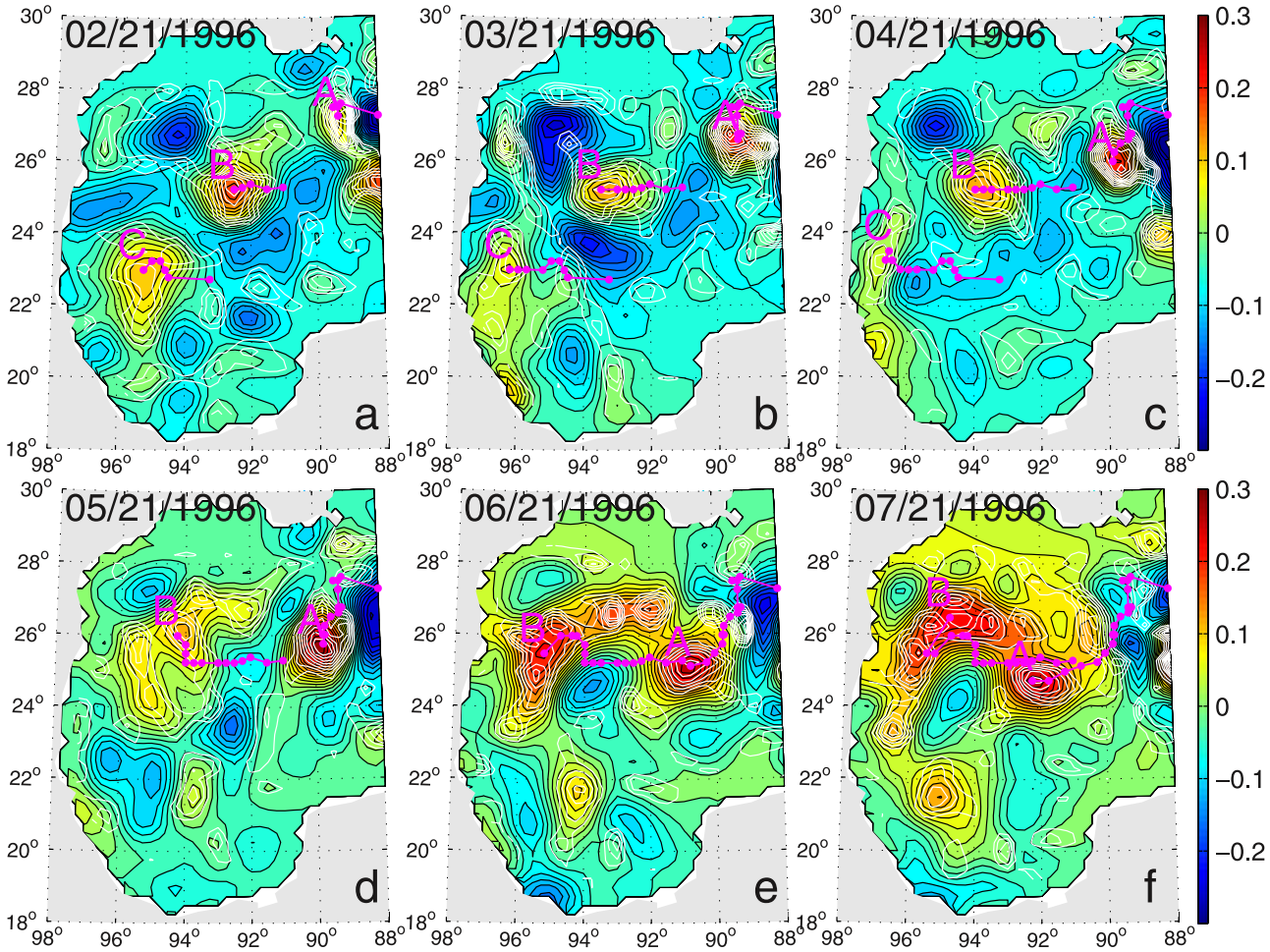

Figure 4. Sea level anomaly (color scale in m) in the western Gulf of Mexico for the period of February–July 1996 superimposed by Okubo-Weiss parameter (W, white contour). Only negative values of W are depicted with the interval of 2×10^{-6} s^{-2}. Trajectory of three major anticyclonic eddies (96A, 96B, and 96C) is depicted every 10 days (white dots) starting at 1 January 1996.

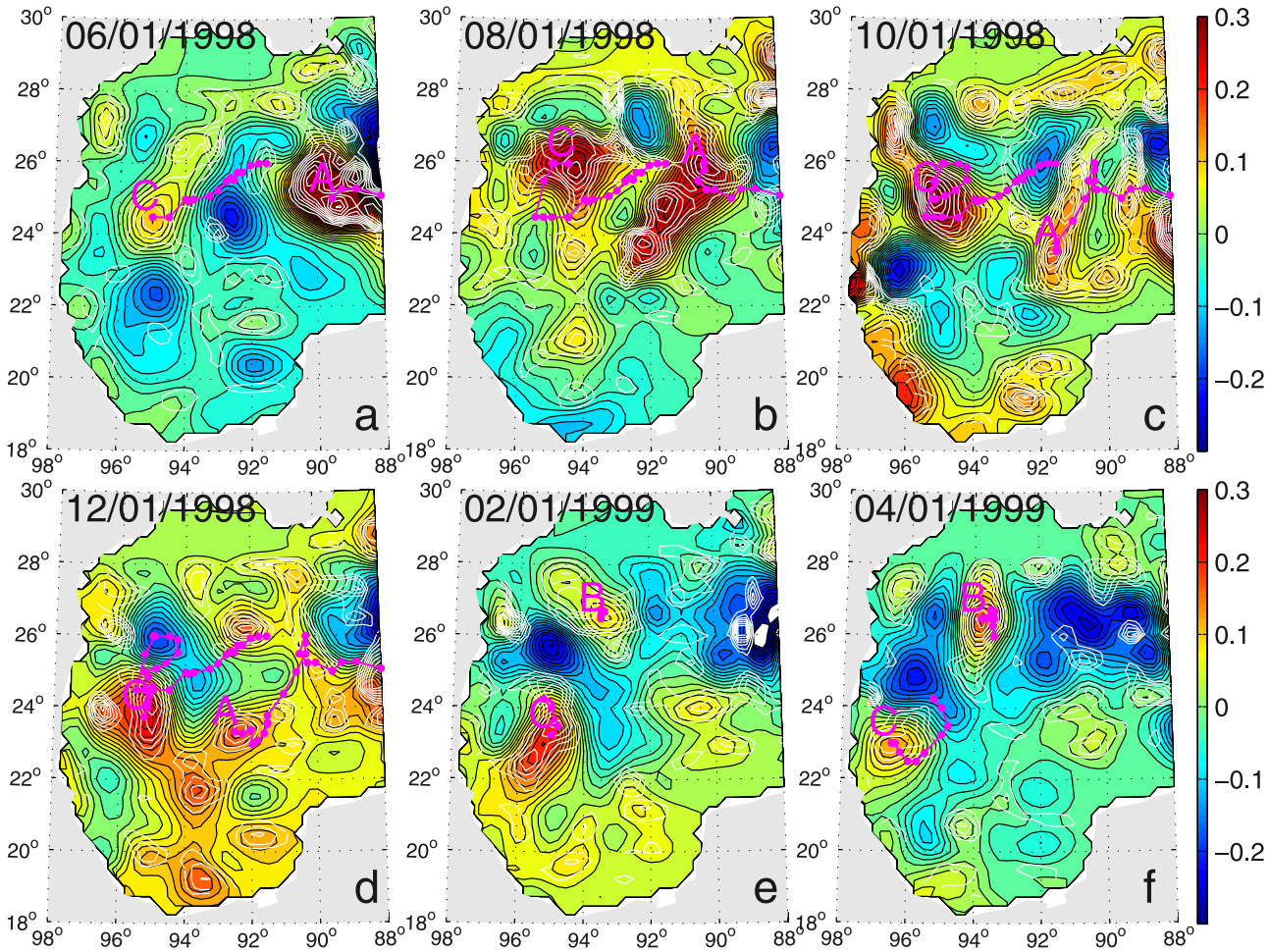

Figure 5. Same as Figure 4, except biomonthly distribution from June 1998 to April 1999 for eddies 98A, 98C, and 99B.

pass the projection at 96W/26N (Figure 5b) (discussed in section 3.2.1).

[15] Figure 5 illustrates two eddies (98C, 98A) which experience eddy–western/northern slope collision. In June 1998 (Figure 5a), 98C is located near the western slope (95W/24.5N) and 98A is about to shed (89.5W/25N). 98C collides with the slope (95.5W/24.5N), reflects northeastward in July (Figure 6b), and subsequently translates eastward and southwestward again, delineating a big anticyclonic (clockwise) route in October (Figure 5c). 98C then collides with the western slope again (second impact) and reflects southeastward (Figures 5d and 5e), and then experiences a third impact (97W/23N) after another large anticyclonic trajectory in April 1999 (Figures 5e and 5f). This eddy well demonstrates the ET collision on the western slope accompanying offshore reflection and anticyclonic drift routes. Eddy 98A, located 89.5W/25.0N in June 1998 (Figure 5a), undergoes northwestward translation and ET collision with the northern slope (Figure 5b), and then southwestward translation after August 1998 (Figures 5b–5f). The northern edge of 98A extending to the shelf break in the northern GOM and anticyclonic trajectory indicates ET collision with the northern slope, resulting in strong eddy distortion and subdivision. Note how the circular shape of 98A in June evolves into a southwest-northeast distorted elliptic shape in August (Figure 5b), and two subdivided anticyclones, one residing along the northern GOM shelf edge with east-west distortion shape and the other extended southwestward in October (Figure 5c). The southward translating eddy collides with the southern slope and reflects offshore (Figure 5d). In addition to ET collision, eddy-eddy interaction, including the cyclone west of 98A in June (Figure 5a) and 98C in the northwestern GOM in August (Figure 5b) play roles in this eddy evolution. In particular, the cyclone blocks the westward path in June–August and deflects 98A toward the north driving ET collision. Recall the combined translation direction of a zonal CA pair is north, but 98A does not translate further north because of the presence of the northern slope where 98A sharply turns south after the eddy–northern slope collision.

[16] In February 2001, three anticyclones are seen in the GOM including a large eddy (01A) shedding in the central gulf (Figure 6). 01A translates northwestward, collides upon the northern slope in April (Figure 6b) and subsequently translates southwestward in June (Figure 6c). During northwestward translation of 01A, a strong cyclone is located to the southwest, but during southwestward translation, a

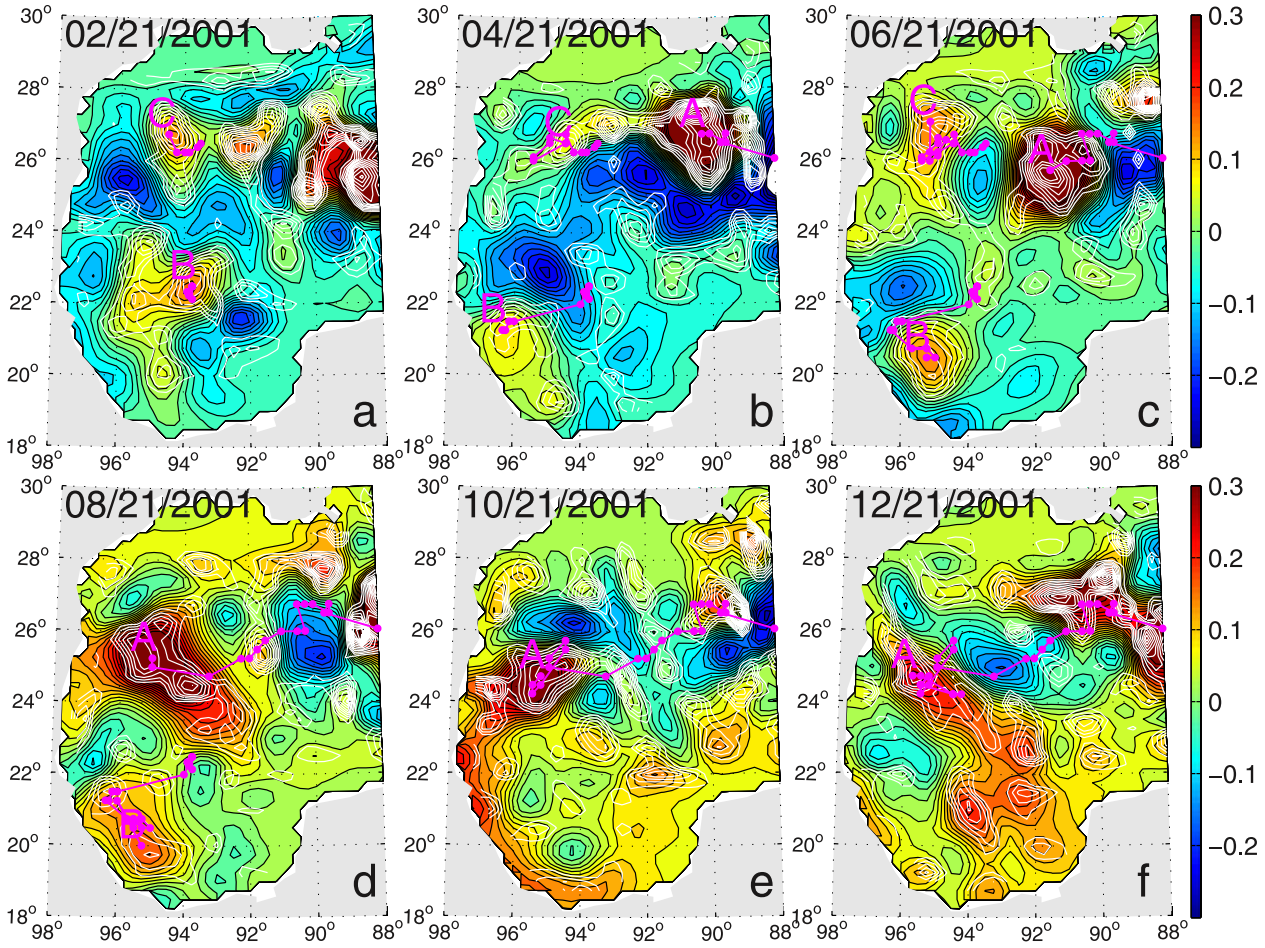

Figure 6. Same as Figure 4, except biomonthly distribution from February to December 2001 for eddies 01A, 01B, and 01C.

strong cyclone is located to the northeast. 01A merges with 01C in August (Figure 6d) and this merged anticyclone collides with the western slope near 95W/25N in August (initial impact), subsequently reflects northeastward (similar to 98C in Figure 5b) and translates southwestward, resulting in an anticyclonic trajectory in October (Figure 6e). 01A collides the western slope near 96W/24.5N again (Figure 6e), subsequently reflecting southeastward (Figure 6f). Two cyclones are seen along the western slope both north and south of 01A, forming a meridional cyclone-anticyclone-cyclone (CAC) triplet. Using hydrographic data *Vidal et al.* [1994] showed that the westward drifting anticyclone colliding against the continental slope generated two flanking cyclones to the north and south and strong southward along-shelf jets, which is quite similar to 01A in December (Figure 6f). In this paper, 98A along with 96A, 01A (Figure 6) are included for examples of eddy−northern slope collision.

[17] A smaller eddy 01B, located at 94W/22.5N in February (Figure 6a), arrives at the southwestern slope (96.5W/21N) in April (Figure 5b), translates southeastward in May (Figure 6c), and finally decays at the southwestern slope (95W/20N) in October. 01B is included as an example which demonstrates eddy−southwestern GOM slope interaction (discussed in section 3.2.4).

[18] According to eddy pathways described from satellite altimetry, zonal translation is dominant in the central GOM and meridional translation frequently occurs near the slopes. In particular, strong southward/northward translation occurs when an LCE collides and interacts with the western and northern slopes. It has been well known that LCEs primarily propagate westward across the central gulf [*Hamilton et al.*, 1999]. The questions are under what situations an LCE translates more southward in the central GOM and how ET collisions alter the path. The LCE path seems affected by various factors, such as eddy-eddy, ET interactions, regional currents and forcing. In this study, the focus is ET interaction, and thus initial eddy-eddy interaction is minimized, and remotely and locally forced currents are absent. In the following sections, results from isolated eddy simulations are presented, and the path and evolution of isolated anticyclones are discussed focusing on ET interactions.

3.2. Topographic Effects on the Evolution of Isolated Eddies

3.2.1. Path of Isolated Eddies in the GOM

[19] Figure 7 depicts 2 year trajectories of the center of isolated anticyclonic eddies (16 cases). Each experiment was performed independently and integrated for 2 model years. In addition to these cases, additional cases with

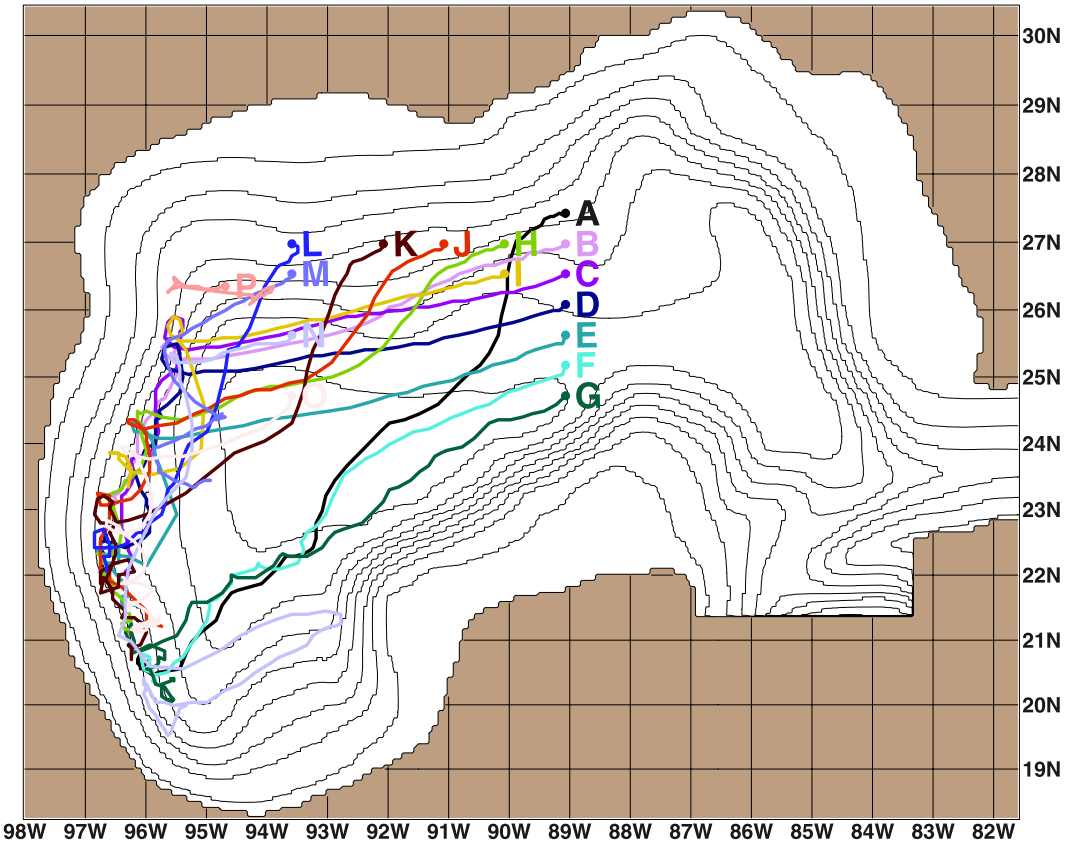

Figure 7. Model bathymetry and trajectories of isolated anticyclonic eddies initialized in the Gulf of Mexico (GOM) with closed boundaries. Trajectory is obtained from the local SSH maximum. Each eddy has the same initial structure (see Figure 1b) except seeding locations. Two year trajectories are depicted except eddy P (270 days). Bathymetry is depicted every 500 m starting from 100 m. Eddy names are denoted near initial locations.

different locations were performed (e.g., along 88W, 90W, 93.5W), but these 16 cases were included in this study because they depict typical eddy paths and ET interactions. Eddies A–G were embedded along 89W between 24.5 and 27.5N; eddies H and I between 26.5 and 27N at 90W; Eddies B, H, J, K, L were embedded on the northern slope along 27N with varying longitude; eddies L, M, N, O, and P were initialized near the western slope. The path of the anticyclones can be divided into three as described below.

[20] Figure 8 illustrates eddy paths and changes in eddy shape and size for all cases. After the initial adjustment, the standard eddy decreases to ~100 km in radius and a relative vorticity of $\sim 0.5 \times 10^{-4}$ s^{-1} while realistic eddies L1 and L2 from a realistic GOM model (Figure 14) have a radius of ~150 km and a relative vorticity of 1.0×10^{-4} s^{-1}. Even though the realistic LCEs are ~1.5 times stronger and bigger than the standard case, they show quite consistent trajectory and evolutions with the standard idealized cases.

[21] Eddies embedded over the northern slope (A, H, J, K) translate alongslope initially, and then southward or southwestward in the central GOM. Eddy A translates alongslope ~1° and turns south at 90W/27N, turns southwest at 90W/25N, and finally reaches the southwestern GOM corner (96W/20.5N). Eddy H translates alongslope ~1° westward, turns southwest at 91W/26.5N, turns west at 93W/25N and propagates westward until it arrives at the western slope (96W/24.5N). Eddy H subsequently tracks 2–3 anticyclonically curved routes and translates southward along the western slope. Eddy J and K follow a trajectory similar to eddy H except for an enhanced southward component.

[22] Eddies B, C, D, E, I in the central gulf translate dominantly westward until they impinge upon the western slope. For example eddy B shows westward trajectory until it arrives at the western slope (95.5W/25N), turns south delineating an anticyclonic route. Eddies C, D, E and I demonstrate a trajectory similar to eddy B, except the initial impact point is located further south.

[23] Eddies F/G, initially located near the Campeche Bank (24.8–25.2N/89W), translate southwestward following the GOM southern slope. Eddy F translates southwestward along the Campeche Bank, turns further south at 92.5W/23.5N, and arrives at the southwestern corner (96W/20.5N), in distinct contrast with eddy E which dominantly drifts westward. Note the initial distance between E and F is 0.5° in latitude but the impact points at the western slope are 4° apart. This result clearly indicates that southward translation is strongly enhanced near the southern continental slope. Eddy G, initialized 0.5° south of eddy F, translates along the Campeche Bank and continuously experiences offshore/onshore oscillation because of ET collision. The oscillatory trajectory is quite an interesting phenomenon, resulting from the competition between the topographic

Figure 8. Evolution of idealized eddies depicted by isostreamlines and trajectory for 2 years except eddy P (240 days). A streamline of 0.5 Sv and maximum values at layer 7 are depicted every 5 days for the eddy shape and trajectory, respectively.

and planetary β effects. Recall that the topographic β effect causes cyclone's onshore tendency and anticyclone offshore reflection while the planetary β effect causes anticyclone's southward translation with a coherent trailing cyclone.

[24] Eddy M, initially located near the northwestern corner (93.5W/26.5N), translates southwestward without alongslope translation, reflects southeastward after impinging at 95.5W/25.5N, and subsequently turns southwest at the deep GOM (95W/24.5N) and experiences a second impact at the western slope (96W/24N). Strong southward translation for A, K, L is analogous to 96A, 98A and 01A shown in Figures 3, 4, and 5 and is due to eddy–northern slope collision (section 3.2.2). Eddies N, O, initialized near the western slope, show that eddies drift mainly westward near the western slope similar to the eddies from the central gulf (e.g., eddies B–E) with a slight stronger collision and reflection. Eddy P, initialized at the northwest corner, shows stationary and dissipative evolution, which is similar to LCE 96b, 99b, 00c shown in Figure 3. Extensive simulations have been performed near the NW corner and showed that 26N is the critical latitude for corner trapped eddies.

3.2.2. Eddy–Northern GOM Slope Collision

[25] This section describes how eddy–northern GOM continental slope interaction enhances southward eddy

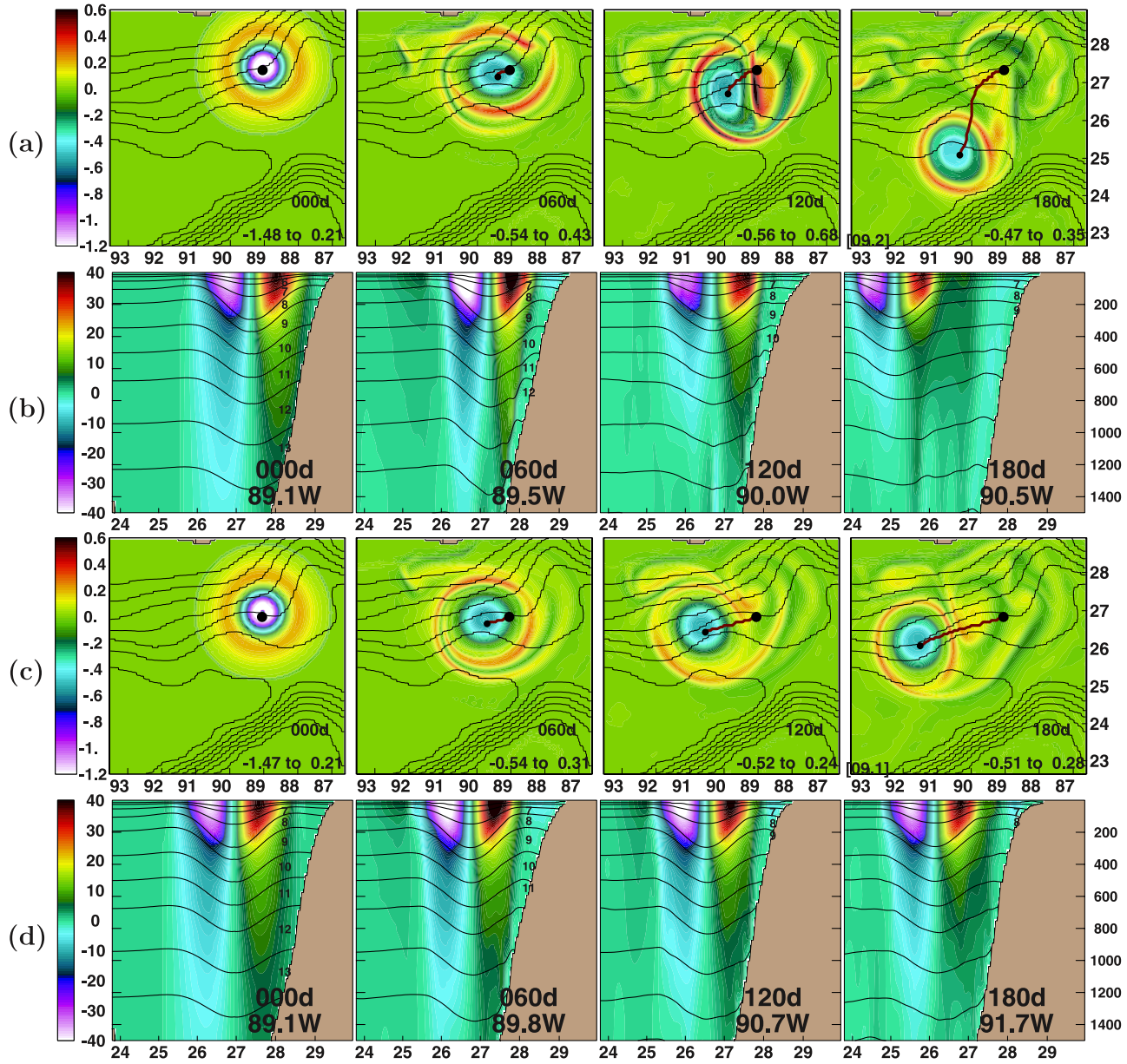

Figure 9. The evolution of (a, b) eddy A and (c, d) eddy B which are initialized in the northeastern GOM. Relative vorticity (ζ) ($\times 10^{-4}$ s^{-1}) at layer 1 and the meridional section of the currents crossing the center of eddy are depicted every 60 days. Dates and maximum/minimum vorticity are denoted in Figures 9a, 9b, 9c, and 9d. Trajectory of the eddy center, obtained from local maximum layer thickness, is denoted red lines with black dots. Bathymetry is superimposed every 500 m from 100 m. Color scale is in units of 10^{-4} s^{-1} for vorticity and cm s^{-1} for currents.

translation and affects the subsequent eddy evolution. Eddies A and B are compared because the initial locations are very close to each other but their trajectories are sharply distinguished. Figure 9 depicts relative vorticity in layer 1 and zonal currents sectioning the eddy center.

[26] Offshore reflection: Both eddies have a cyclonic vorticity rim which mediates the eddy core and the ambient water at rest (see day 0 in Figure 9). As eddy A starts to evolve, the cyclonic vorticity rim interacts with the topography before the eddy core actually make a contact with the topography. Note a narrow striped band of the cyclonic rim north and south of the elliptic eddy A on day 60, which is a signature of the ET interaction (Figure 9a), while eddy B remains relatively circular and the cyclonic rim is weaker (see day 60 in Figure 9c), even though both eddies generate eddy filaments around the core. The ET interaction occurs first in the lower layer where the eddy is being forced in other directions i.e., when the original translation is dragged or blocked by topography. Note eddy A becomes slender more strongly (day 60 in Figure 9b) than eddy B (day 60 in Figure 9d), distorting the vortex in north-south direction (Figure 9a). A difference between eddies A and B is that the vortex column of eddy A directly impinges on the slope (which acts like a lateral boundary) (see day 0 in Figure 9b)

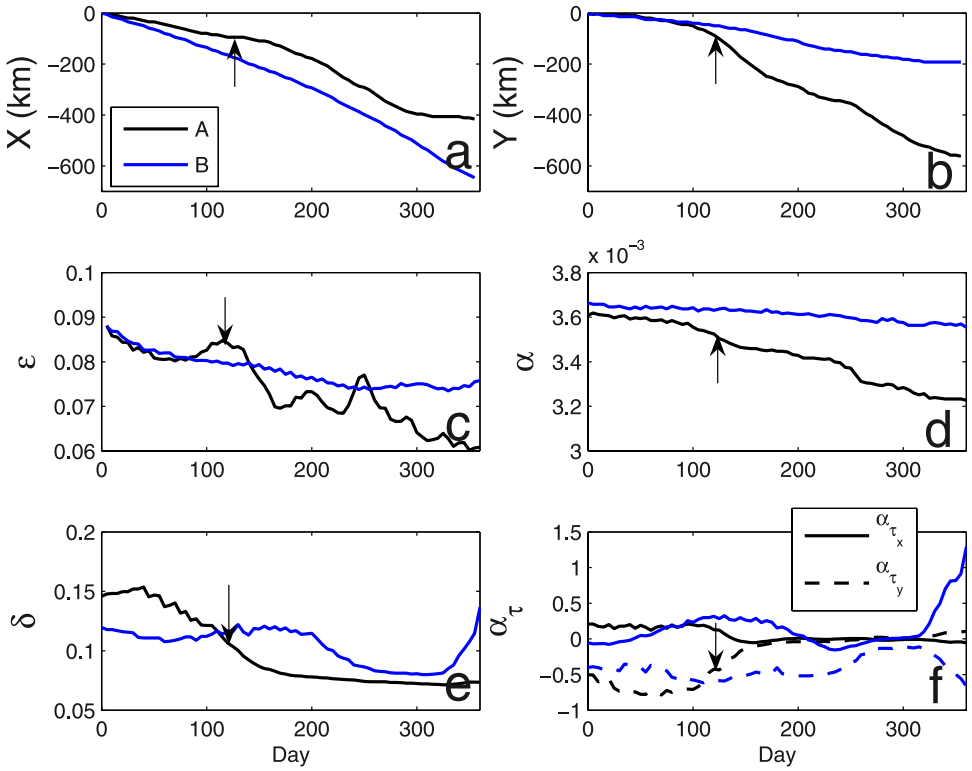

Figure 10. Time series of eddy properties of eddies A (black) and B (blue). (a) Zonal and (b) meridional translation distance, (c) eddy intensity number ε, (d) eddy size number α, (e) eddy barotropy δ, and (f) the topographic effect number α_τ are depicted. Nondimensional numbers are defined in equations (3) and (4) in the text.

but eddy B remains slightly separated from the slope. The distortion of eddy A is similar to *Oey and Zhang* [2004, Figures 5 and 7], who reported the generation of a cyclone and a strong slope jet west of an anticyclone "smashing" onto the northern slope. However, the slope jet is not generated in our experiments, instead it is more likely that the collision strengthens the cyclone to the east (day 120 in Figure 9a) and several slope cyclones propagating westward (see days 120, 150 in Figure 9a). ET collision also strongly enhances eddy erosion, i.e., note eddy A shoals to ~500 m on day 150 from ~1200 m on day 90 (Figure 9b) but that the core thickness of eddy B does not change significantly with time (see Figure 9d).

[27] Dipole: As shown in Figure 9a, a cyclone becomes much stronger east of eddy A (see day 120) as the eddy and the cyclonic vorticity rim swirl clockwise distorting into a north-south direction, forming a dipole. The generation of a dipole can be described by the well-known β-gyre dynamics [*LaCasce*, 1998], and in general it was known that the cyclone was formed in the lower layer by the movement of the upper anticyclone [*Sutyrin et al.*, 2003]. In this study the cyclone is much strengthened by eddy-topography collision and the dipole is very clear in the surface layer, in contrast with eddy B (Figure 9c). Once the cyclone detaches from eddy A after day 180 the eddy turns west (see trajectory in Figure 7), indicating that the strength of the cyclone is critical in the meridional translation. The evolution of eddy A is very similar to the LCEs 96A (Figure 4), 98A (Figure 5), 01A (Figure 6) and a small eddy located at 88.5W/27.5 in June 2001 (Figure 6d). These LCEs smash onto the northern slope from the south during the shedding period, subsequently reflect southwestward, and they are always accompanied by a cyclone to the east. On the basis of the results above, eddy distortion caused by ET collision is a primary factor that enhances the interaction with the trailing cyclone and the subsequent southward reflection.

[28] Figure 10 depicts time series of eddy characteristics of eddies A and B. Zonal/meridional translation is dominant for eddies B/A. Zonal translation is ~1.3 (1.8) km d^{-1} and meridional translation is ~1.8 (0.6) km d^{-1} for eddy A (B) (Figures 10a and 10b). An overall decrease in ε and α indicates eddy intensity and size decrease with time (Figures 10c and 10d). Eddy A dissipates faster than B because of two ET collisions (as shown in Figure 10b), indicating that ET collision strongly enhances the dissipation. During the first ET collision (day 120), eddy A experiences a slight intensity increase but rapid size decrease (Figures 10c and 10d). A simultaneous decrease in δ and absolute value of $\alpha_{(\tau_x,\tau_y)}$ indicates offshore vortex reflection, resulting in reduced zonal and enhanced meridional translation (Figures 10a and 10b). On the other hand the second collision occurs with the southern slope as a "lateral" wall since the eddy center is located in the deep GOM (see consistent δ and $\alpha_{(\tau_x,\tau_y)}$ after day 200).

3.2.3. Eddy–Northwestern GOM Slope Collision

[29] The GOM northwestern slope exhibits topographic characteristics of narrow and steep slope with the slope orientation of southwest-northeast between 24 and 26N and

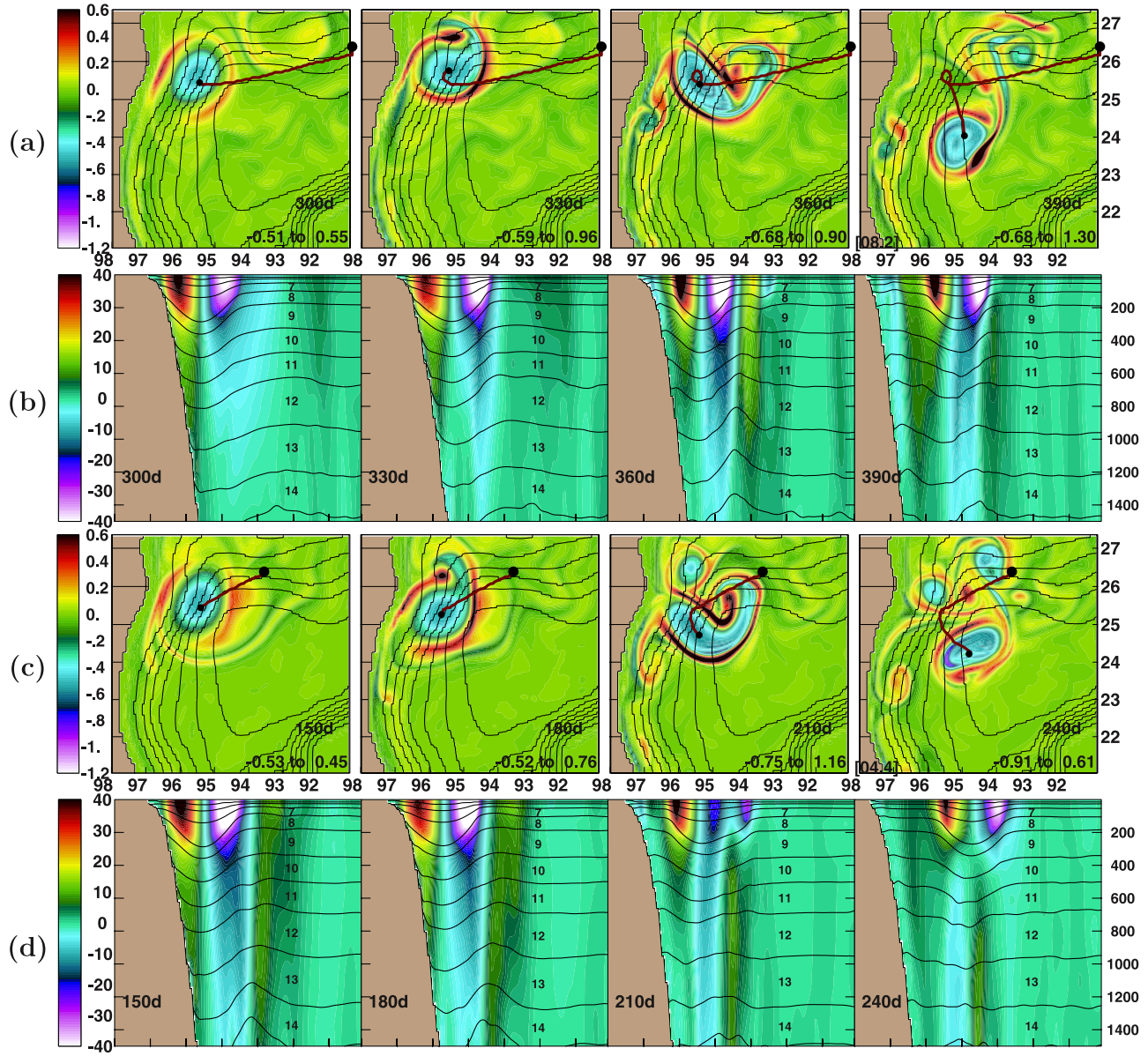

Figure 11. The evolution of (a, b) eddy I and (c, d) eddy M. Figures 11a and 11c show horizontal vorticity field, and Figures 11b and 11d show zonal section of the meridional current (cm s^{-1}) for every 30 days. Otherwise, same as Figure 9.

a corner shape north of 26N. Eddies I and M are chosen to demonstrate eddy–northwestern slope collision (Figure 11) and eddy property variation (Figure 12).

[30] Slope jet and "collision" cyclone: Strong cyclonic filaments (collision cyclone in HH) generated south of the impact propagate southward along the shelf break (Figures 11a and 11c), and a core speed of ~15 cm s^{-1} is detected near the shelf edge (Figures 11b and 11d). The slope jet is the southward branch of the onshore flow of the colliding eddy and can extend vertically to ~1200 m (see day 390 in Figure 11b) and horizontally to the southwest corner (see day 390 in Figure 11a), even though the jet gradually weakens and evolves into isolated slope cyclones (day 390 in Figures 11a and 11c), which is analogous to lower continental slope cyclonic eddies in the central GoM [*Hamilton*, 1992]. The slope jets and slope cyclones occur vigorously on the western slope compared to the northern slope, because of stronger ET collision (e.g., by comparing size and intensity changes in Figures 10 and 12). Southward propagation of the slope cyclones and the slope jets has patterns quite similar to coastally trapped waves propagation as demonstrated by *Zamudio and Hogan* [2008].

[31] Anticyclonic track and dipole: Anticyclonic trajectories are a typical phenomenon generated by ET collision on the western slope [*Sutyrin et al.*, 2003; *Frolov et al.*, 2004a], and are seen two times for eddy I, during the first collision and between southward reflection and the second collision. The anticyclonic trajectory consists of northward translation in the onshore side and southward reflection in the offshore side. Northward translation occurs when the onshore vortex column is overcompressed horizontally and vertically during ET collision (see Figure 11b and HH). Simultaneously

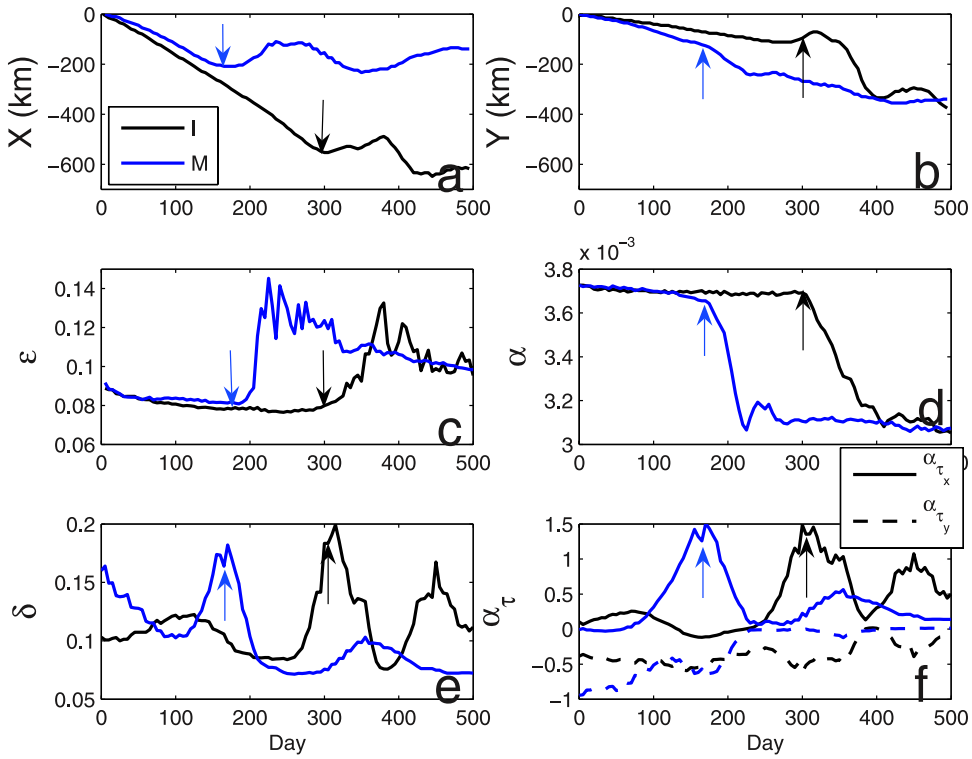

Figure 12. Same as Figure 10 except eddies I (black) and M (blue) as shown in Figure 11. The arrows denote the initial collision point at the GOM western slope.

the topographic β-effect peaks (see Figures 12e and 12f), generating a cyclone to the north (dipole), i.e., note a strong cyclone to the north on day 330 (Figure 11a). This dipole formation and topographic β effect induces vortex offshore advection. The second anticyclonic trajectory is large and closely related with dipole propagation, i.e., eastward translation slows as a cyclone moves southeast of the eddy (day 360 in Figures 11a and 11b) and translates westward with the cyclone located to the south. Subsequently the eddy collides with the slope near 96.5W/24N again. As mentioned previously, even though northwestward/northeastward translation is opposite to the conventional anticyclone translation, it is frequently observed in the northwestern GOM (e.g., 96B in Figure 4, 98C in Figure 5b, and 01A in Figure 6) [*Kirwan et al.*, 1988]. Anticyclonic routes seen in eddy I and eddy L1 from a realistic GOM model (discussed in section 3.3) support that northward migration observed in the western GOM is part of the anticyclonic route promoted by ET collision and dipole propagation. 96B in 1996 (Figure 4), 98C in 1998 (Figure 5), 01C/01A in 2001 (Figure 6) are good examples analogous to eddy I. Specifically, 01C in 2001 demonstrates good agreement, depicting an anticyclonic route over the slope during the initial collision and recollision after southeastward reflection. 98C in 1998 also shows a large anticyclonic trajectory after the second collision (Figures 5e and 5f). Also during a strong southeastward reflection, the cyclone northeast of the anticyclone, which enhances offshore reflection, is consistent with the model results.

[32] Eddy erosion and slope anticyclone: ET collision induces strong eddy erosions horizontally and vertically (HH). Note the enormous decrease in size after the collision (Figure 12d). Eddy M is a good example of the eddy erosion process. Vertically the deep eddy (>1200 m on day 180 in Figure 11d) shoals to 400 m on day 240. Below the surface eddy on day 240, a deep cyclone is formed centering at ~1200 m (Figure 11d). Horizontally, eddy M undergoes subdivision, i.e., it subdivides into small-scale slope anticyclones located in the northwest slope corner (94W/26.5N) and in the northern slope (96W/25.5N) on day 240. These isolated anticyclones gain strength as they translate to the NW corner and form an anticyclone-cyclone-anticyclone (ACA) triad combined with a cyclone in the middle. This ACA triad is quite similar to Figures 15 and 16 in the paper by *Vukovich and Waddell* [1991], who observed the triad during a hydrographic survey in January–May 1986 concurrent with the southeast reflection of an LCE. The LCE named Triton which was cleaved by a cyclone [*Biggs et al.*, 1996, Figure 9] also provides a consistent pattern with the ACA triad in this study.

[33] Eastward reflection: Eastward eddy reflection is caused by the offshore potential vorticity advection due to the maximized topographic β effect during the ET collision. The reflection speed is much faster than the incidence speed, i.e., compare the translation distance between days 360–390 and before (Figure 11a). The eddy reflection magnitude seems to be determined by the collision intensity, the steepness of the impact point (topographic β), the incidence angle and the location of adjacent cyclones. The eddy intensity and incidence speed first determines collision intensity, i.e., a strong and fast drifting eddy induces a strong collision/reflection. For example, eddy B demon-

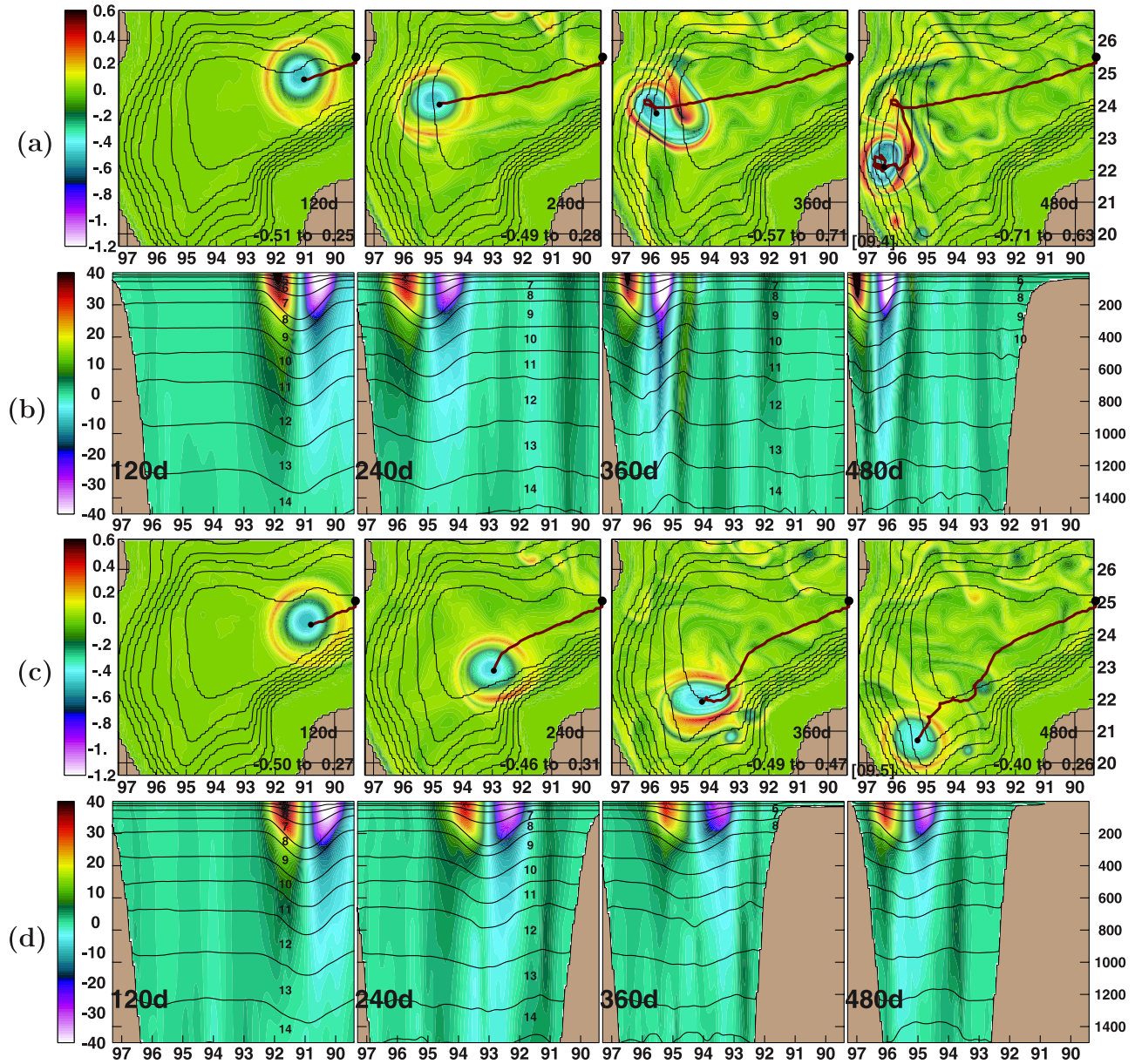

Figure 13. The evolution of (a, b) eddy E and (c, d) eddy F. Otherwise, same as Figure 9.

strates a similar trajectory with eddy I, except for weaker southward reflection (see Figure 7) because the former collides the slope later than the latter (weaker intensity).

[34] Eddies I and M also demonstrate that the angle of incidence is closely related with the angle of reflection. Eddy M, initialized on the northern slope, collides with the northwestern slope on day 180 from the northeast, and reflects southeastward without the anticyclonic route until it sharply turns southwest (Figure 11c). Note the larger incidence and reflection angle for eddy I and vice versa for eddy M. Angles of incidence and reflection are not equal for ET collision; however those angles are very close, particularly when the energy transfer is very small.

[35] Eddy barotropy and topographic β peaks at the collision point (Figures 12e and 12f), yielding a stronger eddy reflection. Recall that the western slope between 24.5 and 25.5°N is steeper than the rest of the western slope and the northern slope. *Frolov et al.* [2004a] investigated the effect of slope width (i.e., slope steepness) on the cyclic path (synonymous with the nomenclature "anticyclonic trajectory" used here) by comparing narrow and wide slopes, and reported that the amplitude of the cyclic path was significantly larger for the narrow slope, which allows the deep cyclonic eddies to form beneath a large portion of the LCE. *Smith* [1986] also discussed the eddy offshore reflection by the ET collision with a strong lower layer rotational strength.

3.2.4. Eddy–Southern/Southwestern GOM Slope Interaction

[36] This section describes the eddy interaction with the southern and southwestern slopes. Initial locations of eddies E, F are very close to each other, but they illustrate very distinct trajectories (Figure 13). Eddy E translates dominantly westward and collides with the western slope (96W/

Figure 14. Temporal variation in SSH (cm) from the GOM model using HYCOM (see text for model details). SSH is depicted every 30 days starting 5 January 2000 for 450 model days. Trajectory of the center of eddies L1 and L2 are marked with white dots and lines every 10 days.

24N) on day ~330, while eddy F reaches the southwestern GOM corner after turning south on day 180 (92W/23.5N), and this difference is associated with the topographic effect of the southern slope. As shown in the eddies initialized in the central gulf (eddies A–E, I), westward drifting eddies do not have a strong trailing cyclone to the east. Please compare the sections on day 240 for both eddies (Figures 13b and 13d), and note that the trailing cyclone substantially strengthens when eddy F turns south on day 240 (Figure 13d), while eddy E translates mostly westward without a trailing cyclone (Figure 13b), and as eddy E turns south a stronger cyclone is present to the east (day 360 in Figure 13b). Before arriving at the western slope, eddy E also is accompanied by a stronger cyclone to the south (a meridional AC pair) during the prevailing westward translation (not shown), which is very similar to eddy 96B in Figure 4. Although not included in this paper, a series of experiments with a flat bottom and realistic coastline geometry with the same initial locations of eddies E, F were performed to examine whether or not the trailing cyclone was coherent to the anticyclone on the flat bottom. Those cases demonstrate southwestward translation with a coherent trailing cyclone, in contrast to prevailing westward translating eddies over the realistic bathymetry, especially in the central GOM. This result indicates that the coherency of the trailing cyclone is critical to eddy translation and that the southern slope tends to "confine" the cyclone once the eddy is sufficiently close to the slope, subsequently resulting in alongslope translation.

[37] The southwestern slope, which has a relatively gentle and wide slope and an orientation of southeast-northwest, is the final destination for most long-lived anticyclones in the GOM. Eddy E, which collides strongly with the slope (96.5W/22N) from the north, tracks an anticyclonic route near 96.2W/22.0N. Eddy F collides relatively gently with the slope (96W/21N) from the east on day 510 and turns south following the slope (see Figure 8). The anticyclonic route indicates that northward migration can be induced by a strong ET collision on the southwestern slope, however, eddy-eddy attractions before the merger (e.g., 96C in Figures 4c and 4d) and other forcing (currents and winds)

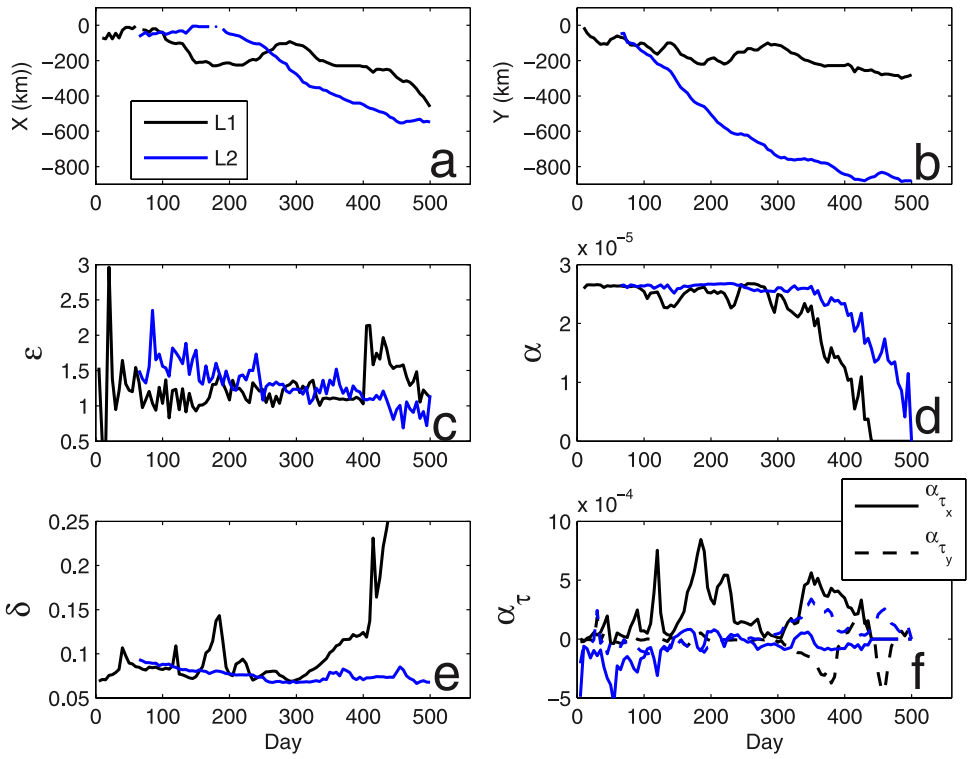

Figure 15. Properties of eddies L1 (black) and L2 (blue) illustrated in Figure 14. Otherwise, same as Figure 10.

also play roles in northward migration. Eddy 98C (Figures 5e and 5f) is very similar to eddy E and eddies 95D, 99E (Figure 3) are analogous to eddy F.

3.3. Comparisons With a Realistic Model

[38] This section describes a result from a realistic GOM model to support the results from the idealized simulations and observations discussed in the previous sections. A realistic HYCOM model with open boundary and initial conditions from an 1/12° North Atlantic HYCOM simulation [see *Chassignet et al.*, 2003] was applied for the GOM domain. Wind and thermal heat flux forcing of NOGAPS [*Hogan and Rosmond*, 1991] for the period of 2000–2001 was applied. Horizontal grid resolution of 1/25° and vertically 20 layers with the KPP vertical turbulence model were utilized. Figure 14 depicts monthly sea surface height (SSH) starting from 5 model days after initialization from the North Atlantic HYCOM and the trajectory of major LCEs (every 10 days denoted as white dots) and Figure 15 depicts eddy property variation.

[39] Eddy L1, initially located near the slope (94W/25N on day 5 in Figure 14), exhibits strong ET interactions, experiencing four ET collision events (see Figure 15c): one at 95.5W/25N on day 35, another at 95W/25N on day 125, another at 96W/24N on day 185 and a fourth collision that is not clearly seen in Figure 14 but is detected in Figure 15e. The first and third collisions generate northward translation (Figure 15b) and the corresponding anticyclonic route, and the third collision generates the strongest reflection (Figure 15e). L1 is a good example to demonstrate the topographic effect of the northwestern slope and is analogous to eddy I (see Figure 11), including two anticyclonic routes, southeastward reflection, the generation of a slope jet and slope cyclones (see days 95, 125). In particular, the initial anticyclonic route is very large compared to eddy I, and the northeastward reflection is clearly seen, which is analogous to observed LCE 98C in Figure 5a.

[40] Eddy L2 takes the alongslope path following the southern slope, which is analogous to eddies F and G (see Figure 7). L2 departs near the Campeche Bank (88W/25N) on day 95, translates westward initially until day 245 and subsequently turns southwest. When L2 turns south (day 275), a cyclone is clearly located to the northeast and continues to trail L2 until it arrives at the southwestern corner. When turning south, L2 experience a rapid shoaling of the eddy core (Figure 15d), indicating the linkage between southward translation and eddy dissipation for potential vorticity conservation. Another LCE, shedding at 88W/25N on day 365, follows a similar trajectory as L2, which provides a good example of southwestward path along the southern slope and topographic effect of the southern/southwestern slopes.

4. Summary

[41] This paper investigates how the bottom topography affects the path and evolution of LCEs in the GOM using the MODAS satellite altimetry and the HYCOM ocean circulation model. The model is applied to simulate idealized anticyclonic eddies initialized at various positions in the GOM with realistic bottom topography and coastline geometry but closed boundaries and to simulate realistic LCE propagation with lateral and surface boundary forcing. On the basis of both satellite data and the model simulations, specific topographic features demonstrate unique topographic effects on the LCE path and evolution:

[42] 1. The northwest eddy collision and southwest reflection against the northern GOM slope frequently occur, and an associated cyclone to the east (significantly strengthened by the collision) forms a dipole, which plays a critical role in the reflection.

[43] 2. In the relatively flat central gulf, eddies translate dominantly westward because the associated trailing cyclone tends to disperse toward nearby topographic features which reduces the southward component of translation, and/or the cyclone moves to the south from the east generating a meridional AC pair which enhances the combined westward translation.

[44] 3. A strong eddy collision normal to the steep northwestern slope occurs around 24–26N and is accompanied by an anticyclonic trajectory, an extensive southeastward reflection, a collision cyclone and a slope jet south of the impact and several slope anticyclones generated by enhanced eddy erosion.

[45] 4. Near the southern GOM slope eddies follow an offshore/onshore oscillatory alongslope pathway because of the continuously coherent trailing cyclone and the competition between topographic and planetary β effects.

[46] 5. For eddies strongly colliding at the southwestern GOM slope, a slight northward migration with an anticyclonic route occurs. For weakly colliding eddies, a dissipated slope-following translation dominates.

[47] 6. In the northwestern GOM slope corner (north of 26N), several quasi-stationary eddies are observed from satellite altimetry, which is reproduced in the model for the eddies embedded north of the eastward slope projection near 96W/26N.

[48] The main points in this paper demonstrate that topographic effects play a major role in the path, and evolution and dissipation of Loop Current Eddies in the GOM. In particular the eddy collision incidence angle and the reflection direction varies with the slope orientation (north, northwest, southwest, south), and that the position of the companion cyclone, strengthened by eddy-topography collision, is critical to the combined translation of an anticyclone-cyclone pair. Although some limitations are inherent in the comparison between idealized eddies and observed LCEs, the general pathways of LCEs and the eddy-topography collision/reflection processes are well reproduced in idealized and realistic numerical experiments. Finally this study only focuses on topographic effects, thus the effects of eddy-eddy interactions, forcing and stratification, eddy size and intensity variation warrant further investigation.

[49] **Acknowledgments.** This paper is a contribution to the 6.1 project "Shelf to Slope Energetics and Exchange Dynamics (SEED)" under program element 601153N and the 6.2 project Coastal Ocean Nesting Studies (CO-NESTS) under program element 601153N, both sponsored by the Office of Naval Research. We thank Alan Wallcraft (NRLSSC) for his contribution in the development of HYCOM and the use of ARSC HPC computers. We thank Steven Herbette (JRC/IES) for providing the source code used for the eddy initialization and Charlie Barron (NRLSSC) for the use of MODAS data. We thank two anonymous reviewers for their constructive comments and suggestions, which greatly improved this paper.

References

Biggs, D. C., G. Fargion, P. Hamilton, and R. Leben (1996), Cleavage of a Gulf of Mexico Loop Current Eddy by a deep water cyclone, *J. Geophys. Res.*, *101*, 20,629–20,641, doi:10.1029/96JC01078.

Bleck, R., and D. Boudra (1981), Initial testing of a numerical ocean circulation model using a hybrid (quasi-isopycnic) vertical coordinate, *J. Phys. Oceanogr.*, *11*, 755–770, doi:10.1175/1520-0485(1981)011<0755:ITOANO>2.0.CO;2.

Carton, X., and J. C. M. McWilliams (1989), Barotropic and baroclinic instabilities of axisymmetric eddies in a quasigeostrophic model, in *Mesoscale/Synoptic Coherent Structures in Geophysical Turbulence*, edited by J. Nihoul and J. Jamart, *Elsevier Oceanogr. Ser.*, *50*, 225–244.

Chassignet, E. P., L. T. Smith, G. R. Halliwell, and R. Bleck (2003), North Atlantic simulation with the HYbrid Coordinate Ocean Model (HYCOM): Impact of the vertical coordinate choice, reference density, and thermobaricity, *J. Phys. Oceanogr.*, *33*, 2504–2526, doi:10.1175/1520-0485(2003)033<2504:NASWTH>2.0.CO;2.

Chassignet, E. P., H. E. Hurlburt, O. M. Smedstad, C. N. Barron, D. S. Ko, R. C. Rhodes, J. F. Shriver, A. J. Wallcraft, and R. A. Arnone (2005), Assessment of data assimilative ocean models in the Gulf of Mexico using ocean color, in *Circulation in the Gulf of Mexico: Observation and Models*, *Geophys. Monogr. Ser.*, vol. 161, edited by W. Sturges and A. Lugo-Fernandez, pp. 87–100, AGU, Washington, D. C.

Fox, D. N., W. J. Teague, and C. N. Barron (2002a), The Modular Ocean Data Assimilation System (MODAS), *J. Atmos. Oceanic Technol.*, *19*, 240–252, doi:10.1175/1520-0426(2002)019<0240:TMODAS>2.0.CO;2.

Fox, D. N., C. N. Barron, M. R. Carnes, M. Booda, G. Peggion, and J. V. Curley (2002b), The Modular Ocean Data Assimilation System (MODAS), *Oceanography (Wash. D.C.)*, *115*, 22–28.

Frolov, S. A., G. G. Sutyrin, G. D. Rowe, and L. M. Rothstein (2004a), Loop Current Eddy interaction with the Western Boundary in the Gulf of Mexico, *J. Phys. Oceanogr.*, *34*, 2223–2237, doi:10.1175/1520-0485(2004)034<2223:LCEIWT>2.0.CO;2.

Frolov, S. A., G. D. Rowe, L. M. Rothstein, and I. Ginis (2004b), Cross-shelf exchange processes and the deep water circulation of the Gulf of Mexico: Dynamical effects of submarine canyons and the interactions of Loop Current Eddies with topography, report, 149 pp., U.S. Dep. of the Inter. Miner. Manage. Serv., New Orleans, La.

Grimshaw, R., D. Broutman, X. He, and P. Sun (1994), Analytical and numerical study of a barotropic eddy on a topographic slope, *J. Phys. Oceanogr.*, *24*, 1587–1607, doi:10.1175/1520-0485(1994)024<1587:AANSOA>2.0.CO;2.

Hamilton, P. (1992), Lower continental slope cyclonic eddies in the central Gulf of Mexico, *J. Geophys. Res.*, *97*, 2185–2200, doi:10.1029/91JC01496.

Hamilton, P., G. S. Fargion, and D. C. Biggs (1999), Loop Current Eddy path in the western Gulf of Mexico, *J. Phys. Oceanogr.*, *29*, 1180–1207, doi:10.1175/1520-0485(1999)029<1180:LCEPIT>2.0.CO;2.

Herbette, S., Y. Morel, and M. Arhan (2003), Erosion of a surface eddy by a seamount, *J. Phys. Oceanogr.*, *33*, 1664–1679.

Herbette, S., Y. Morel, and M. Arhan (2005), Erosion of a surface eddy by a seamount on the β-plane, *J. Phys. Oceanogr.*, *35*, 2012–2030, doi:10.1175/JPO2809.1.

Hogan, P. J., and H. E. Hurlburt (2006), Why do interthermocline eddies form in the Japan/East Sea?, *Oceanography (Wash. D.C.)*, *19*, 134–143.

Hogan, T. F., and T. E. Rosmond (1991), The description of Navy Operational Global Atmospheric Prediction System, *Mon. Weather Rev.*, *119*, 1178–1815, doi:10.1175/1520-0493(1991)119<1786:TDOTNO>2.0.CO;2.

Hurlburt, H. E., and J. D. Thompson (1982), The dynamics of the Loop Current and shed eddies in a numerical model of the Gulf of Mexico, in *Hydrodynamics of Semi-Enclosed Seas*, edited by J. C. J. Nihoul, pp. 243–298, Elsevier, New York.

Hyun, K. H., and P. J. Hogan (2008), Topographic effects on the anticyclonic eddy evolution: A modeling study, *Cont. Shelf Res.*, *28*, 1246–1260.

Isern-Fontanet, J., J. Font, E. García-Ladona, M. Emelianov, C. Millot, and I. Taupier-Letage (2004), Spatial structure of anticyclonic eddies in the Algerian basin (Mediterranean Sea) analysed using the Okubo-Weiss parameter, *Deep Sea Res., Part II*, *51*, 3009–3028, doi:10.1016/j.dsr2.2004.09.013.

Jacob, J., E. Chassignet, and W. Dewar (2002), Influence of topography on the propagation of isolated eddies, *J. Phys. Oceanogr.*, *32*, 2848–2869, doi:10.1175/1520-0485(2002)032<2848:IOTOTP>2.0.CO;2.

Kirwan, A. D., J. K. Lewis, A. W. Indest, P. Reinersman, and I. Quintero (1988), Observed and simulated kinematic properties of Loop Current Rings, *J. Geophys. Res.*, *93*, 1189–1198, doi:10.1029/JC093iC02p01189.

LaCasce, J. H. (1998), A geostrophic eddy over a slope, *J. Phys. Oceanogr.*, *28*, 2362–2381, doi:10.1175/1520-0485(1998)028<2362:AGVOAS>2.0.CO;2.

Large, W. G., J. C. McWilliams, and S. C. Doney (1994), Oceanic vertical mixing: A review and a model with a nonlocal boundary layer parameterization, *Rev. Geophys.*, *32*, 363–403, doi:10.1029/94RG01872.

Lee, H. C., and G. L. Mellor (2003), Numerical simulation of the Gulf Stream System: The Loop Current and the deep circulation, *J. Geophys. Res.*, *108*(C2), 3043, doi:10.1029/2001JC001074.

Mory, M., M. E. Stern, and R. W. Griffiths (1987), Coherent baroclinic eddies on a sloping bottom, *J. Fluid Mech.*, *183*, 45–62, doi:10.1017/S0022112087002519.

Nof, D. (1983), On the migration of isolated eddies with application to Gulf Stream rings, *J. Mar. Res.*, *41*, 399–425.

Nof, D. (1999), Strange encounters of eddies with walls, *J. Mar. Res.*, *57*, 739–761, doi:10.1357/002224099321560555.

Nowlin, W. D., Jr., A. E. Jochens, S. F. DiMarco, R. O. Reid, and M. K. Howard (2005), Low-frequency circulation over the Texas-Louisiana continental shelf, in *Circulation in the Gulf of Mexico: Observations and Model*, *Geophys. Monogr. Ser.*, vol. 161, edited by W. Sturges and A. Lugo-Fernandez, pp. 219–240, AGU, Washington, D. C.

Oey, L.-Y., and H. C. Zhang (2004), The generation of subsurface cyclones and jets through eddy-slope interaction, *Cont. Shelf Res.*, *24*, 2109–2131, doi:10.1016/j.csr.2004.07.007.

Okubo, A. (1970), Horizontal dispersion of floatable particles in the vicinity of velocity singularities such as convergences, *Deep Sea Res. Oceanogr. Abstr.*, *17*, 445–454.

Operational Oceanography Group (2006), Global Temperature-Salinity Profile Program, http://www.nodc.noaa.gov/GTSPP/, Natl. Oceanogr. Data Cent., Silver Spring, Md.

Prasad, T. G., and P. J. Hogan (2007), Upper-ocean response to Hurricane Ivan in a 1/25 nested Gulf of Mexico HYCOM, *J. Geophys. Res.*, *112*, C04013, doi:10.1029/2006JC003695.

Reznik, G. M., and R. Grimshaw (2001), Ageostrophic dynamics of an intense localized vortex on a β-plane, *J. Fluid Mech.*, *443*, 351–376, doi:10.1017/S0022112001005468.

Sansón, L. Z., and G. J.F. van Heijst (2000), Interaction of barotropic eddies with coastal topography: Laboratory experiments and numerical simulations, *J. Phys. Oceanogr.*, *30*, 2141–2162, doi:10.1175/1520-0485(2000)030<2141:IOBVWC>2.0.CO;2.

Shi, C., and D. Nof (1993), The splitting of eddies along boundaries, *J. Mar. Res.*, *51*, 771–795, doi:10.1357/0022240933223927.

Smith, D. C., IV (1986), A numerical study of Loop Current interaction with topography in the western Gulf of Mexico, *J. Phys. Oceanogr.*, *16*, 1260–1272, doi:10.1175/1520-0485(1986)016<1260:ANSOLC>2.0.CO;2.

Smith, D. C., IV, and J. J. O'Brien (1983), The interaction of a two-layer isolated mesoscale eddy with bottom topography, *J. Phys. Oceanogr.*, *13*, 1681–1697, doi:10.1175/1520-0485(1983)013<1681:TIOATL>2.0.CO;2.

Sturges, W., and A. Lugo-Fernandez (Eds.) (2005), *Circulation in the Gulf of Mexico: Observation and Models*, *Geophys. Monogr. Ser.*, vol. 161, 347 pp., Washington, D. C.

Sutyrin, G. G., G. D. Rowe, L. M. Rothstein, and I. Ginis (2003), Baroclinic eddy interaction with continental slopes and shelves, *J. Phys. Oceanogr.*, *33*, 283–291, doi:10.1175/1520-0485(2003)033<0283:BEIWCS>2.0.CO;2.

Teague, W. J., M. J. Carron, and P. J. Hogan (1990), A comparison between the generalized digital environmental model and Levitus climatologies, *J. Geophys. Res.*, *95*, 7167–7183, doi:10.1029/JC095iC05p07167.

Thierry, V., and Y. G. Morel (1999), Influence of a strong bottom slope on the evolution of a surface intensified eddy, *J. Phys. Oceanogr.*, *29*, 911–924, doi:10.1175/1520-0485(1999)029<0911:IOASBS>2.0.CO;2.

Vidal, V. M.V., F. V. Vidal, and J. M. Perez-Molero (1992), Collision of a Loop Current anticyclonic ring against continental slope of the western Gulf of Mexico, *J. Geophys. Res.*, *97*, 2155–2172, doi:10.1029/91JC00486.

Vidal, V. M.V., F. V. Vidal, A. F. Hernandez, E. Meza, and J. M. Perez-Molero (1994), Baroclinic flows, transports, and kinematic properties in a cyclone-anticyclone-cyclone triad in the Gulf of Mexico, *J. Geophys. Res.*, *99*, 7571–7598, doi:10.1029/93JC03334.

Vukovich, F. M. (2005), Climatology of ocean features in the Gulf of Mexico: Final report, *OCS Study MMS 2005-031*, 58 pp., U.S. Dep. of the Inter. Miner. Manage. Serv., New Orleans, La.

Vukovich, F. M., and B. W. Crissman (1986), Aspects of warm rings in the Gulf of Mexico, *J. Geophys. Res.*, *91*, 2645–2660, doi:10.1029/JC091iC02p02645.

Vukovich, F. M., and E. Waddell (1991), Interaction of a warm ring with the western slope in the Gulf of Mexico, *J. Phys. Oceanogr.*, *21*, 1061–1074, doi:10.1175/1520-0485(1991)021<1062:IOAWRW>2.0.CO;2.

Weiss, J. (1991), The dynamics of enstrophy transfer in two-dimensional hydrodynamics, *Physica D*, *48*, 273–294, doi:10.1016/0167-2789(91)90088-Q.

Zamudio, L., and P. J. Hogan (2008), Nesting the Gulf of Mexico in Atlantic HYCOM, *Ocean Modell.*, *21*, 106–125, doi:10.1016/j.ocemod.2007.12.002.

P. J. Hogan, Naval Research Laboratory, Code 7323, Stennis Space Center, MS 39529, USA.

K. H. Hyun, Department of Marine, Earth, and Atmospheric Sciences, North Carolina State University, Raleigh, NC 27695, USA. (khyun@ncsu.edu)